

X-RAY SPECTRAL SHAPE VARIATIONS IN CHANGING-LOOK SEYFERT GALAXY SDSSJ155258+273728

YANLI AI¹, LIMING DOU^{2,3}, CHENWEI YANG^{4,5}, LUMING SUN^{5,6}, FU-GUO XIE⁷, SU YAO⁸, XUE-BING WU^{8,9}, TINGGUI WANG^{5,6}, XINWEN SHU¹⁰

Draft version December 3, 2019

ABSTRACT

We analyze the X-ray, optical, and mid-infrared data of a Seyfert galaxy SDSS J155258+273728 at $z \simeq 0.086$. The broad H α line intensity increased by a factor of ~ 4 in a decade. Accompanied with this, the X-ray emission detected by *Chandra* was about five times brighter than that from *Suzaku* in 2010, and the corresponding V-band, mid-infrared W1 band brighten $\sim 0.18, 0.32$ mag, respectively. The X-ray spectrum flattens in the *Chandra* bright state with a photon index of $1.52^{+0.06}_{-0.06}$, compared to the value of $2.03^{+0.22}_{-0.21}$ in the *Suzaku* low state. Only moderate absorption was detected in all the X-ray observations with $N_{\text{H}} \sim 10^{21} \text{cm}^{-2}$. The accretion rate of SDSS J155258+273728 is low with an Eddington ratio below a few percent, suggesting that the inner region of the accretion disk is possibly a hot accretion flow. By compiling the X-ray data from literatures, we find that “changing-look” AGNs generally follow the well-studied correlation shape (“V-shape”) in AGNs, that is, above a critical turn-over luminosity the X-ray spectra soften with the increasing luminosity, and below that luminosity the trend is reversed in a way of “harder when brighter”. This presents direct evidence that CL-AGNs have distinctive changes in not only the optical spectral type, but also the X-ray spectral shape. The similarity of the X-ray spectral evolution between CL-AGNs and black hole X-ray binaries in their outbursts indicates that the observed CL-AGNs phenomena may relate to the accretion state transition.

Subject headings: galaxies: active — quasars: general — quasars: emission lines — accretion, accretion disks

1. INTRODUCTION

The optical/UV continuum variability of AGNs/quasars on timescales of months to years with typical fluctuations of $\simeq 10\%$ has long been known and was well studied in recent years with wide-area, multi-epoch optical surveys (e.g. Vanden Berk et al. 2004; Ai et al. 2013; Li et al. 2018; Sun et al. 2018). This continuous and stochastic variability is mostly explained in the context of standard accretion disk theory with different scenarios, i.e., reprocessing of emission from near the black hole (e.g. McHardy et al. 2014; Edelson et al. 2019), local instabilities on thermal timescale (e.g. Kelly et al. 2009; Cai et al. 2016,

2018), or changes of global mass accretion rate with confinement of viscous timescale (e.g. Liu et al. 2016). Well-sampled spectroscopic monitoring has shown that the variability in broad emission line fluxes well correlated with that of continuum as “light echoes”, and the delay measured with “reverberation mapping” technique is used to probe the structure and kinematics of the line-emitting gas (e.g. Kaspi et al. 2005; Peterson 2014; Du et al. 2018; Shen et al. 2016).

Extreme spectroscopic and photometric variability is detected in a small fraction of AGNs, which are intriguing for investigation of changes of accretion states in proximity to black hole and circumnuclear gas. Large optical luminosity variations by factor of $\gtrsim 2$ were detected in quasars (e.g. Lawrence et al. 2016; Rumbaugh et al. 2018; Graham et al. 2019). Disappearing or appearing broad Balmer emission lines have been known for many years in a number of local low-luminosity AGNs (e.g. Tohline & Osterbrock 1976; Cohen et al. 1986; Denney et al. 2014; Shappee et al. 2014). With large-scale time-domain survey recent studies have identified a growing number of such cases in quasars with associated large, order of magnitude variations in optical continuum on month to year timescales (LaMassa et al. 2015; MacLeod et al. 2016; Ruan et al. 2016; Runco et al. 2016; Runnoe et al. 2016; Stern et al. 2018; Wang et al. 2018; Yang et al. 2018; MacLeod et al. 2019; Sheng et al. 2019; Trakhtenbrot et al. 2019). Their optical classification was caught to change between type 1.8-2 (narrow-line) to type 1 (broad-line) AGN (or vice versa), and even from low-ionization nuclear emission-line region galaxy (LINERs) to broad-line quasars (Gezari et al. 2017; Frederick et al. 2019). These ob-

¹ School of Physics and Astronomy, Sun Yat-Sen University, Guangzhou 510275, China, aiyanni@mail.sysu.edu.cn

² Center for Astrophysics, Guangzhou University, Guangzhou 510006, China

³ Astronomy Science and Technology Research Laboratory of Department of Education of Guangdong Province, Guangzhou 510006, China

⁴ Antarctic Astronomy Research Division, Key Laboratory for Polar Science of the State Oceanic Administration, Polar Research Institute of China, Shanghai, China.

⁵ School of Astronomy and Space Sciences, University of Science and Technology of China, Hefei, China.

⁶ Key Laboratory for Research in Galaxies and Cosmology of Chinese Academy of Sciences, Department of Astronomy, University of Science and Technology of China, Hefei, China.

⁷ Key Laboratory for Research in Galaxies and Cosmology, Shanghai Astronomical Observatory, Chinese Academy of Sciences, 80 Nandan Road, Shanghai 200030, China

⁸ Kavli Institute for Astronomy and Astrophysics, Peking University, Beijing 100871, China

⁹ Department of Astronomy, School of Physics, Peking University, Beijing 100871, China

¹⁰ Department of Physics, Anhui Normal University, Wuhu, Anhui, 241000, China

jects were known as “changing-look active galactic nuclei” (CL-AGNs hereafter). The first case with dramatic diminishment of Mg II in one CL-AGN was reported in Guo et al. (2019).

Recent evidences from Spectropolarimetry (e.g. Hutsemékers et al. 2019), mid-infrared echo (Sheng et al. 2017) imply that variable obscuration is a rather unlikely explanation for the CL-AGNs. The drastic spectral changes seen in CL-AGNs most plausibly come from the intrinsic changes in accretion power. The timescales, from months to years, relevant for the CL-AGNs reported up until now, are far shorter than what is expected for global accretion rate changes in the standard think disk (e.g., Stern et al. 2018). Different models are proposed to address the timescale problem, while all clearly make out that dramatic variations take place at the inner radius of accretion gas are responsible for the changing-look phenomena, either from disk instability or a switch in the nature of accretion flow, or both (Ross et al. 2018; Stern et al. 2018; Noda & Done 2018; Dexter et al. 2019a; Dexter & Begelman 2019b; Śniegowska & Czerny 2019).

CL-AGNs may be naturally accounted for if they were experiencing the state transition analogous to X-ray binaries. Studies of the correlation between the UV-to-X-ray spectral index and Eddington ratio of CL-AGNs have revealed the possible similarities to the spectral evolution of outbursting X-ray binaries (Ruan et al. 2019a,b). For the two CL-AGNs, Mrk 590 and Mrk 1018, soft X-ray excess disappeared during decay, similarly to the soft-to-hard state transition in X-ray binaries (Rivers et al. 2012; Noda & Done 2018). More multi-band monitoring of CL-AGNs, specifically in X-ray, will provide clues about the physics process occurred in the region proximity to black holes.

The Seyfert galaxy, SDSS J155258+273728 at $z \simeq 0.086$, was recently identified as “turn-on” CL-AGN with significantly increased broad H α line emission (Yang et al. 2018). This object was classified as Seyfert 1.9 in Osterbrock (1981) with only weak broad H α emission line. We present mid-infrared, optical to X-ray photometric and spectral monitoring data of the source from 2006-2018 (section 2). From the multi-bands variability analysis we confirm that CL-AGNs are powered by intrinsic variations in accretion power (section 3). We probe the X-ray spectral evolution for CL-AGNs and provide clear evidence that the X-ray spectral shape changes with the optical spectral types transition (section 4). Our results indicate that the CL-AGNs phenomena are mostly related with or driven by accretion state transitions.

2. OBSERVATIONS

We proposed spectroscopic observation with Double spectrograph (DBSP) of the Hale 200-inch telescope, and *Swift* observation in 2018. The object was also observed with *Suzaku* in 2010, and *Chandra* in 2014. We summarize the data sets and reduction procedures used here.

2.1. Optical spectra

SDSS J155258+273728 was observed by SDSS on 2005 May 8 through a diameter 3'' fiber over the wavelength range 3800-9200 Å at a spectral resolution of $\simeq 2000$ (Abazajian et al. 2009). The spectrum, with relatively

weak emission lines, is dominated by the host galaxy starlight emission (Figure 1). The object was included in the LAMOST quasar survey with spectroscopic observation on 2014 March 5 (Ai et al. 2016; Dong et al. 2018; Yao et al. 2019). LAMOST is a 4 meter reflecting Schmidt telescope equipped with 4000 fibers of 3'' diameter each (Zhao et al. 2012). The wavelength coverage ranges from 3700 Å to 9000 Å with overall spectral resolution of $\simeq 1800$. The LAMOST spectrum was scaled to match the red spectrum with the blue spectrum. Compared to SDSS, the significant feature in LAMOST spectrum is the prominent broad H α emission line, as shown in Figure 1.

SDSS J155258+273728 was followed up with the optical Double spectrograph (DBSP) of the Hale 200-inch telescope at Palomar Observatory (P200) on 2018 February 24. Observation was taken through a 1.0'' slit width, using a D55 dichroic, a 600/4000 grating for the blue side, and a 316/7500 grating for the red side. The grating angles were adjusted to obtain a nearly continuous wavelength coverage from 3300 to 10000 Å except for a small gap of 5500–5550 Å. The data were reduced following the standard routine. The spectrum was extracted with a 2'' aperture and flux calibrated using the standard star. The significant broad H α line is also clearly shown in the DBSP spectrum (Figure 1).

2.2. Optical spectral fitting

To compare the strengths of emission lines among different observations, we recalibrated LAMOST and DBSP spectra with that of SDSS assuming the [O III] $\lambda 5007$ line is not variable over a timescale of 10 yr. As shown in Figure 1, the spectra of SDSS J155258+273728 are dominated by host galaxy starlight rather than the emission from active nucleus itself in all the three epochs. We first fit a starlight model to the SDSS spectrum to constrain the stellar component. Prior to fitting, all spectra were shifted back to the rest-frame and corrected for Galactic extinction.

We fit the SDSS spectrum with the BC03 stellar population model Bruzual & Charlot (2003) using the STARLIGHT code Cid Fernandes et al. (2005). In the fitting we masked all the prominent emission lines. The resulting starlight model matched the continuum well and no extra non-stellar component is needed (Figure 1). We then scaled the starlight model from SDSS to match the spectra in DBSP and LAMOST with scale factors chosen by minimization of the residuals in the stellar continuum and absorption lines. For both DBSP and LAMOST spectra, there are also no additional power-law component from the AGN continuum required. We then fit the emission lines in the residual spectra.

Gaussian function is used to model the emission lines and we generally follow the method in Ai et al. (2016) with only minor modifications. The H α emission line was modelled with one narrow and one broad component. The broad component is fitted with three Gaussians. The velocity offsets and line widths of [N II] $\lambda\lambda 6548, 6584$ and [S II] $\lambda\lambda 6717, 6731$ are tied to those of H α narrow component. The relative flux ratio of the two [N II] components is fixed to 2.96. The upper limits of the full width at half-maximum (FWHM) for the narrow lines are set to be 1200 km s $^{-1}$. No broad component was detected in

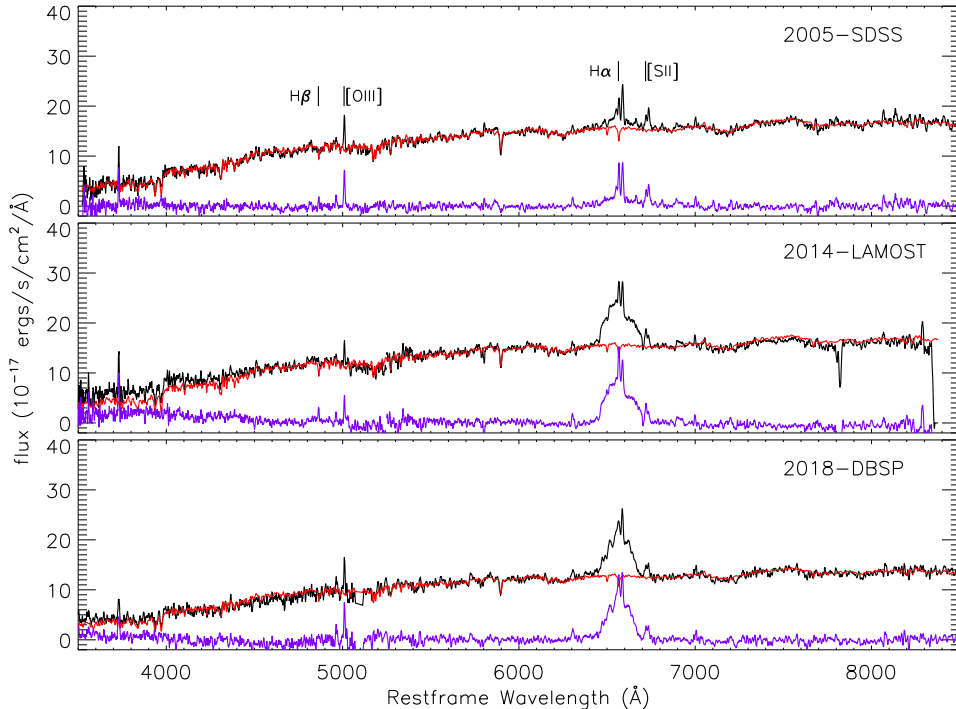


FIG. 1.— Optical spectra of SDSS J155258+273728. The black curves show the observed spectra, the red curves show a host galaxy starlight template that was fit to the SDSS spectrum and scaled to LAMOST and DBSP spectra. The purple curves show the residuals with starlight components subtracted from the observed spectra.

the $H\beta$ line in all of three observations. Thus we model the $H\beta$ line with only one narrow component. Each line of the $[O\text{ III}] \lambda\lambda 4959, 5007$ doublet is modelled with one Gaussian, and the doublet are assumed to have the same redshifts and profiles, with flux ratio fixed to the theoretical value of 3. Velocity offsets and line widths of the doublet core component are tied to those of narrow $H\beta$ component. The fitted models, along with individual components, for the $H\alpha$ and $H\beta$ emission lines in different epochs, are shown in Figure 2. The parameters are summarized in Table 1. Dramatic change occurs in the broad $H\alpha$ line between 2005 and 2014/2018. The uncertainties quoted for each parameter are calculated through 10^3 Monte Carlo simulations of each spectrum based on their 1σ flux density uncertainties. The spectral fitting procedure is performed for each spectrum, and 1σ spread in the resulting distributions of resampled parameters are reported as uncertainties.

2.3. X-ray observations and data reduction

Suzaku observed SDSS J155258+273728 on 2010 July 31 with exposure of ~ 61 ks. We reduced the data with the HEASOFT software package (v6.21), following the procedure outlined in the *Suzaku* Data Reduction Guide (v5.0). To extract science products from the XIS units, we reprocessed the unfiltered event files for each of the operational CCDs (XIS0,1, 3) and editing modes (3x3, 5x5). Cleaned event files were generated by running the *Suzaku* *aepipeline* pipeline with the latest calibration and screening criteria files (XIS caldb v20160607). The data in the back-illuminated CCD (XIS1) was not used due to the high background level.

SDSS J155258+273728 was also targeted on 2014 December 13 with *Chandra* for ~ 84 ks (PI: Kaastra) us-

ing the Advanced CCD Imaging Spectrometer (ACIS) instrument. We processed the data with standard CIAO version 4.7 and only events with grades of 0, 2, 3, 4, and 6 were considered in the analysis.

SDSS J155258+273728 was clearly detected in both *Suzaku* and *Chandra* observations. In *Suzaku* XIS images, there are two other peaks identified, each at $\sim 150''$ away from SDSS J155258+273728. These two sources are also detected in the *Chandra* image. With the excellent spatial resolution of *Chandra* ACIS the emissions from these two peaks are well constrained, and both of them are about two orders of magnitude fainter than SDSS J155258+273728. In *Suzaku* observation the X-ray spectral shape extracted from the circle with inclusion of all the three peaks is nearly the same with that extracted from with only inclusion the peak of SDSS J155258+273728. Thus we conclude that the X-ray emission of SDSS J155258+273728 dominates in the field of *Suzaku* XIS image. While, to get a clean spectrum, we restrict spectral extraction region to a small circle with radius of a $80''$, corresponding to encircled energy of $\sim 60\%$ ¹¹. The background was extracted from adjacent regions free of any contaminating sources, with care taken to avoid the calibration sources in the corners. Response matrices and ancillary response files were produced with *xisrmfgen* and *xissimarfgen*. Using the FTOOL ADDAS-CASPEC we combine the spectra and response files for the two front-illuminated detectors (XIS0, 3). The combined spectrum was grouped with at least 10 counts in each energy bin.

For *Chandra* ACIS data we extract the source spectrum from a $3''$ circular region. The source spectrum, back-

¹¹ https://heasarc.gsfc.nasa.gov/docs/suzaku/prop_tools/suzaku_td/node9.html

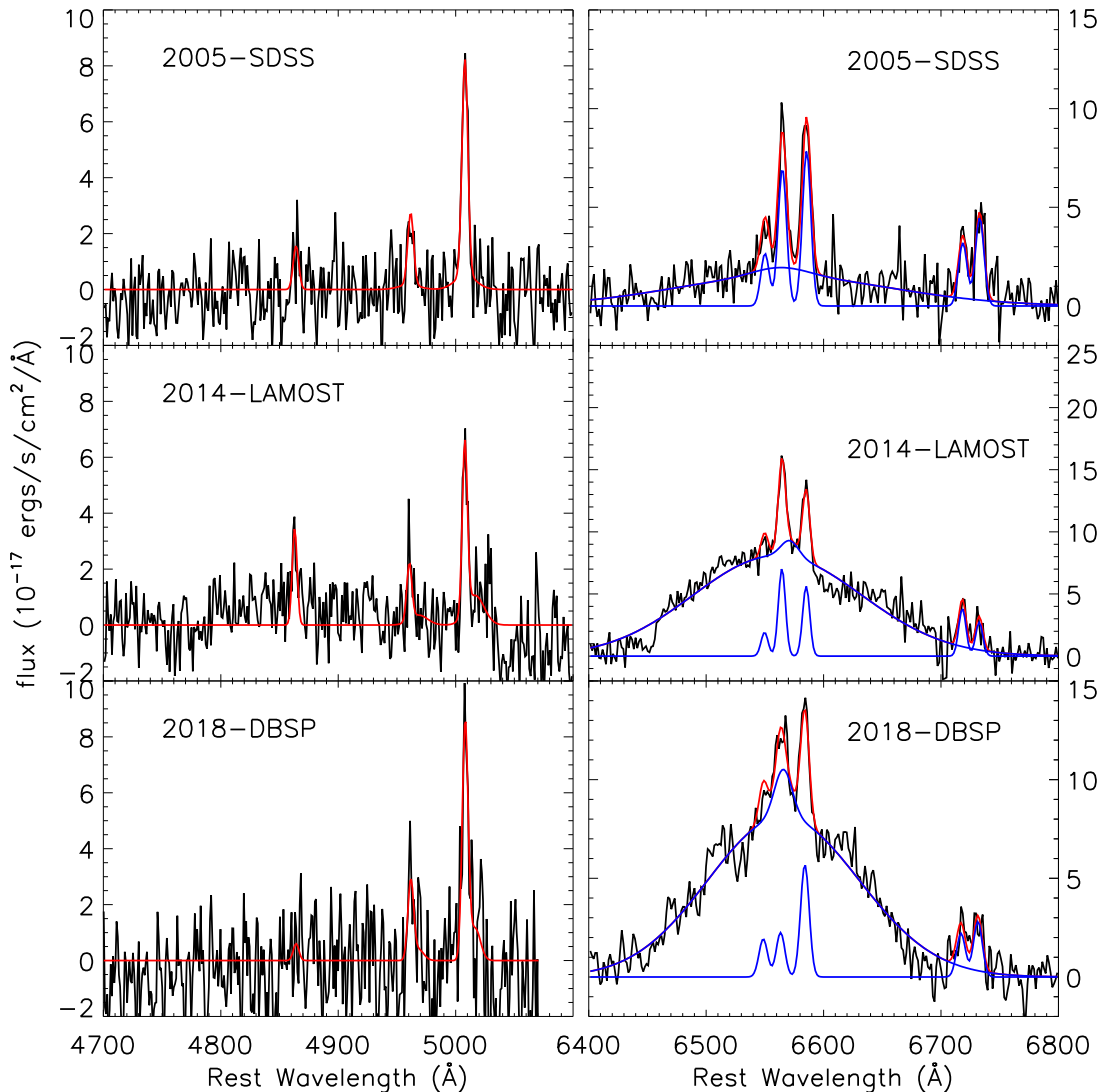


FIG. 2.— Starlight-subtracted spectra of SDSS J155258+273728 zoomed to exhibit H β and H α emission-line region. The combination of models (red) and individual components (blue) are shown.

ground spectrum, response matrix files, and auxiliary matrix files are built using the CIAO script SPECEXTRACT. The *Chandra* spectrum was grouped with 15 counts per bin.

We requested and were granted a 2 ks *Swift* X-ray Telescope (XRT) observation on 2018 March 28 for SDSS J155258+273728. There are three archival XRT observations (ObsID: 00611599000-2) with total exposure of 24 ks from 2014 September 3 to Sep 5, of which SDSS J155258+273728 happened to be in the field of view. The XRT observations were processed with the UK Swift Data Science Centre pipeline, which takes into account dead columns and vignetting to extract counts from the source in the energy range of 0.3-10 keV. We combined the three spectra in 2014 as no significant variability was detected between the observations. The X-ray count rate in 2014 and 2018 is 0.0029 ± 0.0003 , 0.0048 ± 0.0017 counts s^{-1} , respectively. We group the XRT spectra with 10 and 2 counts in each energy bin for the 2014 and 2018 epochs.

3. X-RAY SPECTROSCOPY

We fit the X-ray spectra of SDSS J155258+273728 using XSPEC (v12.9, Arnaud (1996)). A simple power-law model modified by Galactic absorption with N_H of $3.02 \times 10^{20} cm^{-2}$ (Kalberla et al. 2005) is applied to all spectra at first. The fit is acceptable for *Suzaku* spectrum, while for *Chandra* spectrum the residuals at soft energy bands less than 1 keV require additional absorption. We then fold the model with intrinsic absorption (at $z = 0.086$). The improvement is significant with $\Delta\chi^2$ of 33 and the fit is acceptable. We also investigate other features in *Chandra* spectra, which has the highest S/N ratio among the four epochs. There are some residuals at energy ~ 7 keV. We then add one Gaussian emission line to fit the feature, while the improvement is not significant. There are no more features that warrant more warm absorption or reflection modelling. We then fit all the spectra with an absorbed power-law model.

The required additional absorption at redshift of the source in *Chandra* spectra modelling is moderate with fitted absorption of $N_H = 12.16^{+3.25}_{-3.05} \times 10^{20} cm^{-2}$. The value of the inferred absorption in *Suzaku* is consistent

TABLE 1
PARAMETERS OF EMISSION LINES FITS^a

	2005–SDSS		2014–LAMOST		2018–DBSP	
	Flux	FWHM	Flux	FWHM	Flux	FWHM
			Broad Lines			
H α	357.9 \pm 22.0	7736 \pm 1992	1461.1 \pm 53.7	6838 \pm 897	1345.6 \pm 34.3	5410 \pm 642
H β	<87.7	...	<70.6	...	<64.6	...
			Narrow Lines			
H α	62.9 \pm 5.8	386 \pm 21	53.6 \pm 16.8	326 \pm 59	19.7 \pm 17.8	397 \pm 40
H β	9.5 \pm 2.8	351 \pm 50	18.1 \pm 14.9	304 \pm 227	3.4 \pm 5.7	350 \pm 134

^a Observed flux in units of 10^{-17} erg cm $^{-2}$ s $^{-1}$ and FWHM in units of km s $^{-1}$.

with that within uncertainties (table 2). The *Chandra* spectra is harder with photon index of $1.52^{+0.06}_{-0.06}$, compared to the value of $2.03^{+0.22}_{-0.21}$ in *Suzaku*. The two *Swift* spectra are even harder than that of *Chandra*, while the value of the photon index can not be well constrained due to low S/N and degeneracy with absorption. Thus in the fitting of *Swift* spectra we tied all the parameters to those of *Chandra* except the normalization. The fitted parameters are shown in table 2, and the spectra with fitted power-law model are shown in Figure 3.

There is more than a factor of 2 brightening in *Chandra* observation with unabsorbed 2–10 keV flux of $6.96^{+0.61}_{-0.72} \times 10^{-13}$ erg s $^{-1}$ cm $^{-2}$, compared to those in *Suzaku* and *Swift*-2014 with values of $1.31^{+0.49}_{-0.37} \times 10^{-13}$ erg s $^{-1}$ cm $^{-2}$, $2.31^{+1.09}_{-0.82} \times 10^{-13}$ erg s $^{-1}$ cm $^{-2}$, respectively. The inferred flux of *Swift*-2018 is $2.74^{+1.58}_{-1.56} \times 10^{-13}$ erg s $^{-1}$ cm $^{-2}$, indicating that the X-ray emission of SDSS J155258+273728 fades back to the level of *Swift*-2014.

3.1. IR-optical-Xray photometry and variability

In Figure 4 we show the X-ray and broad H α line variations of SDSS J155258+273728 on a decade. The optical and mid-infrared photometry from CRTS and WISE survey are also shown. It is clear that accompanied with the significant enhancement of broad H α emission, SDSS J155258+273728 presents increased emission in hard X-ray, optical V-band and mid-IR. The variation timescale of this broad-bands brightening is ~ 4 years, in which the X-ray varied more than a factor 2, and CRTS V-band, mid-IR W1, W2 bands varied with amplitudes of 0.18 ± 0.12 , 0.32 ± 0.02 , 0.43 ± 0.03 , respectively.

4. DISCUSSION

4.1. Reddening measurement from optical spectra

The detected moderate absorption in X-ray indicates that there might be obscurations in our line of sight, possibly accounting for the very weak/undetected continuum emission and broad H β line in SDSS J155258+273728. We follow the procedures described in Trippe et al. (2010) to measure the upper limit of broad H β emission, and to determine if the component should be visible in the spectrum in the absence of reddening. A template representing the intrinsic emitted H β line was made with the broad component of H α at each epoch. We scaled the H α in width to make up for the velocity width difference at H β (Greene & Ho 2005), and divided its flux by 3.0. This template was then added to the

spectrum at the position of H β . For SDSS spectrum, the expected intrinsic H β is indiscernible against the noise, that is, the broad H β line would not be visible even if the broad line regions were totally unreddened. The result indicates that the undetected broad H β line in SDSS spectra may be due to the intrinsic weakness or dust reddened, or both.

For the LAMOST and DBSP spectra, the addition of the template made a visible broad H β line, indicating that H β emission would be observable at these two epochs in the absence of reddening. We then multiple the template with progressively smaller scale factors until the line became indistinguishable. The scale factor times the intrinsic expected H β flux was then taken as an upper limit to the amount of broad H β emission. We show the results in Table 1. The inferred Balmer decrements are steep with values $\lesssim 20.6$, indicating significant dust reddening to the broad emission line regions. To determine the reddening of the BLR, we assumed the intrinsic ratio of the broad components of H α and H β to be equal to $f_{H\alpha}/f_{H\beta} = 3.0$ (Veilleux & Osterbrock 1987; Dong et al. 2008). With assumption of the standard Galactic reddening curve $R(\lambda)$ of Fitzpatrick & Massa (1999) we calculate the reddening using the equation

$$E(B - V) = \frac{2.5}{R_{H\alpha} - R_{H\beta}} \log \frac{3.0}{\frac{f_{H\alpha}}{f_{H\beta}}} \quad (1)$$

The low limit of the $E(B - V)_{BLR}$ is 1.63 for these two epochs.

Such extinction might account for the undetected nuclear continuum in the optical spectra. The observed flux would dim more than two orders of magnitude at the rest wavelength of 5100Å if the central nuclear emissions are also obscured. In the GALEX and *Swift* near- and far-ultraviolet bands SDSS J155258+273728 was not detected. We estimate the rest-frame monochromatic luminosity at 2500Å with the empirical relation of $L_{2500\text{\AA}}$ vs. $L_{2\text{keV}}$ in AGNs (Lusso et al. 2010). Although the inferred intrinsic UV luminosity, $L_{2500\text{\AA}} = 2.02 \times 10^{28}$ erg s $^{-1}$ Hz $^{-1}$, is normal in AGNs, the extinction derived from Balmer decrements makes the object under detection limits in the GALEX and *Swift* observations.

The dust-to-gas ratio in SDSS J155258+273728 is $E(B - V)/N_H \gtrsim 4.31 \times 10^{-22}$ mag cm 2 , somewhat larger than the average Galactic value, 1.7×10^{-22} mag cm $^{-2}$. This indicates that the intrinsic Balmer decrements might be slightly greater than the assumed value of

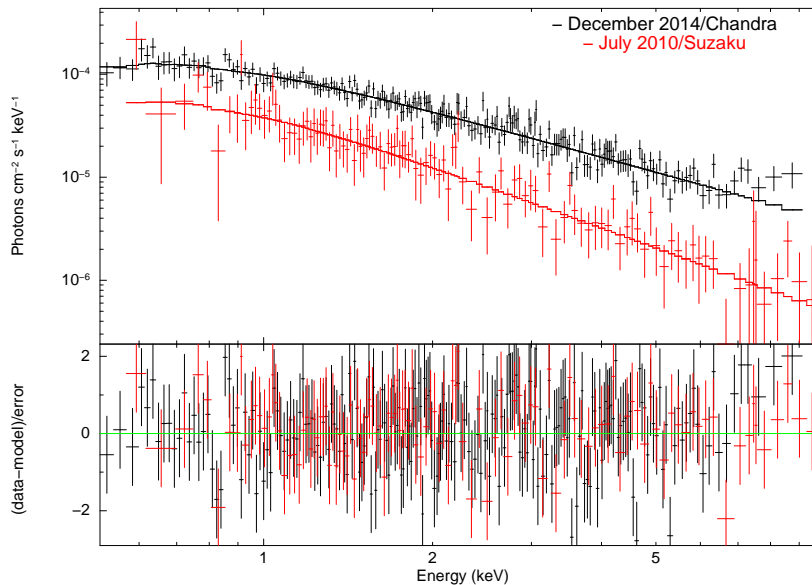


FIG. 3.— Unfolded X-ray spectra of SDSS J155258+273728 with absorbed power-law model fits for *Suzaku* and *Chandra* observations.

TABLE 2
PARAMETERS OF X-RAY SPECTRA FITS^a

Satellite	Date of Obs.	N_{H} (10^{20} cm^{-2})	Γ	$F_{2-10} \text{ keV}^a$ ($10^{-13} \text{ erg s}^{-1} \text{ cm}^{-2}$)
Suzaku	2010.07	$14.07^{+16.22}_{-13.83}$	$2.03^{+0.22}_{-0.21}$	$1.31^{+0.49}_{-0.37}$
Swift	2014.09	12.16*	1.52*	$2.31^{+1.09}_{-0.82}$
Chandra	2014.12	$12.16^{+3.25}_{-3.05}$	$1.52^{+0.06}_{-0.06}$	$6.96^{+0.61}_{-0.72}$
Swift	2018.03	12.16*	1.52 *	$2.74^{+1.58}_{-1.56}$

^a Unabsorbed flux in 2-10 keV.

* The values are fixed in the fitting.

3.0 (e.g., Schnorr-Müller et al. 2016), or there is a higher-than-Galactic dust/gas ratio in the object.

4.2. black hole mass and accretion rate

We estimate black hole mass of SDSS J155258+273728 by virtue of the empirical relation of M_{BH} in AGNs with $L_{\text{H}\alpha}$ luminosity and FWHM of broad $\text{H}\alpha$ line (Greene & Ho 2005). Extinction correction, with the above inferred value, was applied to the broad $\text{H}\alpha$ flux. The measured black hole mass is similar between SDSS and DBSP epochs ($\sim 2.1 \times 10^8 M_{\odot}$), somewhat smaller than that from LAMOST epoch ($\sim 3.5 \times 10^8 M_{\odot}$). The consistent black hole masses from SDSS and DBSP are from the fact that the inferred $\text{H}\alpha$ line becomes narrower in the brighter state (Table 1). The variations of $\text{H}\alpha$ line followed the “breathing” pattern, in which the broad line width decreased by a factor of 1.42, almost identical to $(L_{\text{H}\alpha, \text{SDSS}}/L_{\text{H}\alpha, \text{DBSP}})^{-0.27}$, i.e., 1.43 (Greene & Ho 2005). While, the $\text{H}\alpha$ profile inferred from LAMOST spectrum somewhat deviates from this BLR “breathing” pattern. Such difference is mostly due to the calibration issues in LAMOST spectrum. Thus in this paper we take the black hole mass as $\sim 2.1 \times 10^8 M_{\odot}$.

We estimate the bolometric luminosity of SDSS J155258+273728 with 2-10 keV X-ray luminosity using a bolometric correction factor of 15.8

(Vasudevan & Fabian 2007; Netzer 2019). The Eddington ratio, $L_{\text{bol}}/L_{\text{Edd}}$, of this object is relatively small, with value of 0.007 in the high state at Chandra epoch, and 0.001 in the low state at Suzaku epoch. Such low Eddington ratios suggest that the inner region of the accretion flow is not a cold accretion disk, but instead possibly a hot optically-thin one (Yuan & Narayan 2014).

4.3. Nature of the variability

As discussed above, the central region of SDSS J155258+273728 is most likely obscured. The prominent broad $\text{H}\alpha$ line brightening may be due to the passing out of the obscurers in our line of sight. While, the observed optical/MIR variability amplitudes and timescales provide strong evidences against the predictions from this scenario. First, if the variability is caused by changing of obscuration, any detectable variability in mid-IR bands means a much larger amplitude of variability in optical. For SDSS J155258+273728 the maximum variation in W1 band is ~ 0.51 mag, then $\Delta V \sim 11$ mag is required when assuming the extinction model of Fitzpatrick & Massa (1999). This is significantly larger than what we see in Figure 4.

The other evidence against the variable obscuration scenario is related with time scale. The argument, as

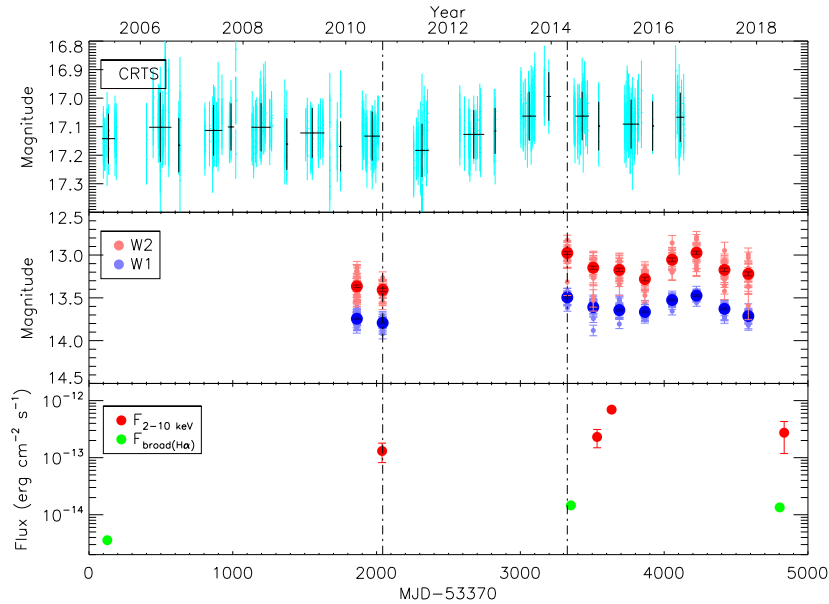


FIG. 4.— Light curves showing the multi-wavelength changes observed in SDSS J155258+273728 in optical V-band data from CRTS (top panel), mid-IR *W1* and *W2* bands from WISE (middle panel), and hard X-ray flux along with broad H α emission (bottom panel). In top and bottom panel, we also present the median values of each season epoch. The dot-dashed lines mark the start/end of the significant variation timescale.

widely discussed in literatures (e.g. LaMassa et al. 2015; Sheng et al. 2017), is that the estimated crossing time for an intervening object orbiting outside the BLR on a Keplerian orbit is longer than the variation timescale of broad Balmer lines and mid-IR emission. The crossing time for the obscuring object is measured as $t_{\text{cross}} = 0.07[r_{\text{orb}}/(\text{lt} - \text{day})]^{3/2} M_8^{1/2} \arcsin(r_{\text{src}}/r_{\text{orb}})$ year, where r_{orb} is the orbital radius of the foreground object, M_8 is the black hole mass in units of $10^8 M_\odot$, and r_{src} is the true size of the obscured region (i.e., the continuum emitting region or the BLR size, LaMassa et al. 2015). In the measurement we adopt the r_{src} as the BLR size, which is estimated from the R- L_{5100} , L_{5100} - $L_{\text{H}\alpha}$ relation (Greene & Ho 2005). The size of the obscurer, r_{orb} , should be at least comparable to the torus to block the hot dust, from which mid-IR emission at 3.4 and 4.6 μm mainly originated. We take the inner radius of the torus as r_{orb} , which was estimated simply from the dust sublimation radius ($R_{\text{sub}} = 0.5L_{46}^{0.5}(1800\text{K}/T_{\text{sub}})$ pc = 0.098 pc). For SDSS J155258+273728 the derived value of t_{cross} is ~ 15.8 yr, which is longer than the significant variation timescale (~ 4 yr).

Thus the dramatic H α line increments seen in SDSS J155258+273728 most plausibly come from the intrinsic changes of the accretion power. The X-ray emission provides a clue to investigate the variations of the accretion. For SDSS J155258+273728 the X-ray spectral shape varied luminosity. In the X-ray high state at *Chandra* epoch the spectrum is harder with $\Gamma = 1.52 \pm 0.06$, compared to that, $\Gamma = 2.03^{+0.22}_{-0.21}$, in the low *Suzaku* state. Correlated variations between X-ray spectral shape and luminosity have been well studied in black hole X-ray binaries (BHBs) and AGNs, with “harder when brighter” found at luminosity below a turning point (e.g., Kalemci et al. 2005; Wu & Gu 2008; Gu & Cao 2009; Sobolewska et al. 2011; Younes et al. 2011; Yang et al. 2015; Connolly et al. 2016), which is around a few percent of the Eddington luminosity, and

above the turning point the spectra then soften as the flux increases (e.g. Wang et al. 2004; Risaliti et al. 2009; Trakhtenbrot et al. 2017). Unlike BHBs, most AGNs only stay in one branch because of small variation in X-ray luminosity of individual sources, the only exception to our knowledge is the low luminosity AGN NGC 7213 (Xie et al. 2016). Such transition in the evolution of X-ray spectral shape is normally interpreted as a consequence of the change in accretion mode, i.e. the region proximity to the black hole varies between a hot accretion flow and a two-phase accretion flow (either numerous cold clumps embedded in a hot flow, or at even higher luminosities a cold thin disk, sandwiched by hot coronas) (Gardner & Done 2013; Qiao & Liu 2013; Xie et al. 2016; Yang et al. 2015). In this picture, the hot accretion flow represents the hard state, the two-phase accretion represents the intermediate state, and the disk-corona configuration is for the soft state (Yang et al. 2015).

Indeed, state transition scenario for CL-AGNs has already been proposed, although the on-off timescale in CL-AGNs remains a challenging task (Noda & Done 2018; Dexter & Begelman 2019b). Based on broad-band continuum spectral modelling Noda & Done (2018) suggests that Mrk 1018 underwent a soft-to-hard state transition as it fades from Seyfert 1 to 1.9. Ruan et al. (2019a,b) claimed that the correlation between the UV-to-X-ray spectral index and Eddington ratio in CL-AGNs is similar to the spectral evolution of BHBs. These results are intriguing, while, we notify that the method of broad-band continuum spectral modelling is only applicable to few individuals due to limited data, and the UV-to-X-ray spectra index can not be well constrained at low state due to the dominated host galaxy emission.

To statistically study the variations of accretion flow in CL-AGNs we compiled the X-ray data from literatures (Longinotti et al. 2007; Denney et al. 2014; LaMassa et al. 2015; Noda & Done 2018; Parker et al. 2019). The result of the relation between hardness ra-

tio, $F_{\text{soft}}/(F_{\text{soft}} + F_{\text{hard}})$, and Eddington scaled hard X-ray luminosity, $L_{X,2-10\text{keV}}/L_{\text{Edd}}$, was shown in Figure 5. Here the F_{soft} and F_{hard} are the absorption corrected flux in soft (0.3-2 keV) and hard (2-10 keV) bands, respectively. We find that for CL-AGNs the hardness ratio increases with luminosity, while, at accretion rates below $L_{X,2-10\text{keV}}/L_{\text{Edd}} \sim 10^{-3}$, there seems to be a turn-over of the relation. We also plot the fits to the relation from previous samples of low-luminosity AGNs by Constantin et al. (2009) and, at higher accretion rates, from Risaliti et al. (2009) with the conversion of Γ to hardness ratio and an assumed bolometric correction factor of $L_{\text{bol}}/L_x = 16$. As shown in the figure, the distributions of CL-AGNs generally follow the well-studied correlation shape (“V”-shape) in AGNs, that is, above a critical turn-over luminosity the X-ray spectra soften with increasing luminosity, and below that luminosity the trend is reversed in a way of “harder when brighter”. However, more data are needed to verify the behaviour of CL-AGNs at accretion rates lower than $L_{X,2-10\text{keV}}/L_{\text{Edd}} \sim 10^{-3}$. In Figure 5 there is also a clear trend that as the optical spectral state fades from type 1 to type 1.9/2, the X-ray spectral shape transits from soft to hard. Our results provide direct evidences on that, the changes in the optical spectral type of CL-AGNs associate with the changes in the X-ray spectral shape transition. In a more aggressive way, these results further indicate that the observed features in CL-AGNs are driven by state transition in accretion physics (see also Noda & Done 2018; Dexter & Begelman 2019b).

5. CONCLUSION

We present multi-bands spectra and variability studies of the changing-look AGN SDSS J155258+273728. We

find:

- Prominent broad H α line was still detected in the recent 2018-DBSP spectra. The steep Balmer decrements indicate our line of sight might be obscured, which possibly account for the very weak/undetected continuum nuclear emission and broad H β line.
- The object presents significant variations in X-ray, optical, and mid-infrared bands. Timescales and amplitudes in these multi-bands variations provide strong evidences against the variable obscurations scenario, indicating intrinsic emission varied in this CL-AGN.
- The X-ray spectral shape varied with the luminosity in a way of “harder when brighter”. In a compiled studies of CL-AGNs we find that the hardness ratio increases with luminosity, while, at accretion rates below $L_{X,2-10\text{keV}}/L_{\text{Edd}} \sim 10^{-3}$, there seems to be a turn-over of the relation. There is also evidence that changes in the optical spectral type associate with the changes in the X-ray spectral shape transition. This similarities of the X-ray spectral evolution to outbursting X-ray binaries support the accretion state transition scenarios of CL AGNs.

Future studies to more CL AGNs with high S/N multi-bands data will provide more clues about the accretion physics happened at the region proximity to central black holes.

REFERENCES

- Abazajian, K. N., Adelman-McCarthy, J. K., Agüeros, M. A. et al. 2009, *ApJS*, 182, 543
- Ai, Y. L., Yuan, W., Zhou, H., et al. 2013, *AJ*, 145, 90
- Ai, Y. L., Wu, X.-B., Yang, J., et al. 2016, *AJ*, 151, 24
- Arnaud K. A., 1996, in Jacoby G. H., Barnes J., eds, *ASP Conf. Ser. Vol. 101, Astronomical Data Analysis Software and Systems V*. Astron. Soc. Pac., San Francisco, p. 17
- Bruzual, G. & Charlot, S. 2003, *MNRAS*, 344, 1000
- Cai, Z. Y., Wang, J. X., Gu, W. M., et al. 2016, *ApJ*, 826, 7
- Cai, Z. Y., Wang, J. X., Zhu, F. F., et al. 2018, *ApJ*, 855, 117C
- Cid Fernandes, R., Mateus, A., Sodré, L., Stasińska, G., & Gomes, J. M. 2005, *MNRAS*, 358, 363
- Cohen, R. D., Rudy, R. J., Puetter, R. C., Ake, T. B., & Foltz, C. B. 1986, *ApJ*, 311, 135
- Connolly, S. D., McHardy, I. M., Skipper, C. J., Emmanoulopoulos, D. 2016, *MNRAS*, 459, 3963C
- Constantin, A., Paul, G., Tom, A., et al. 2009, *ApJ*, 705, 1336
- Denney, K. D., De Rosa, G., Croxall, K., et al. 2014, *ApJ*, 796, 134
- Dexter, J., Xin, S., Shen, Y., et al. 2019a, arXiv:1906.10138
- Dexter, J., & Begelman, M. C. 2019b, *MNRAS*, 483, L17
- Dong, X., Wang, T., Wang, J., et al. 2008, *MNRAS*, 383, 581
- Dong, X. Y., Wu, X.-B., Ai, Y. L., et al. 2018, *AJ*, 155, 189
- Du, P., Zhang, Z. X., Wang, K., et al. 2018, *ApJ*, 856, 6
- Edelson, R., Gelbord, J., Cackett, E., et al. 2019, *ApJ*, 870, 123
- Frederick, S., Gezari, S., Graham, M. J., et al. 2019, arXiv:1904.10973
- Fitzpatrick, E. L., & Massa, D. 1999, *ApJ*, 525, 1011
- Gardner E., & Done C., 2013, *MNRAS*, 434, 3454
- Gezari, S., Hung, T., Cenko, S. B., et al. 2017, *ApJ*, 835, 144
- Graham, M. J., Ross, N. P., Stern, D., et al. 2019, arXiv:1905.02262
- Greene, J. E., & Ho, L. C. 2005, *ApJ*, 630, 122
- Guo, H. G., Sun, M. Y., Liu, X., et al. 2019, arXiv: 1908.00072
- Gu M., & Cao X., 2009, *MNRAS*, 399, 349
- Hutsemékers, D., Agís González, B., Marin, F. et al. 2019, *A&A*, 625, A54
- Kelly, B. C., Bechtold, J., Siemiginowska, A. 2009, *ApJ*, 698, 895
- Kalberla P. M. W., Burton W. B., Hartmann D., et al. 2005, *A&A*, 440, 775
- Kalemci, E., Tomsick, J. A., Buxton, M. M., et al. 2005, *ApJ*, 622, 508
- Kaspi, S., Maoz, D., Netzer, H., et al. 2005, *ApJ*, 629, 61
- LaMassa, S. M., Cales, S., Moran, E. C., et al. 2015, *ApJ*, 800, 144
- Lawrence A., Bruce, A. G., MacLeod, C., et al., 2016, *MNRAS*, 463, 296
- Li, Z. F., McGreer, I. D., Wu, X. B., et al. 2018, *ApJ*, 861, 6L
- Liu, H., Li, S. L., Gu, M. F., Guo, H. X. 2016, *MNRAS*, 462, 56
- Longinotti, A. L., Bianchi, S., Santos-Lleo, M., et al. 2007, *A&A*, 470, 73
- Lusso, E., Comastri, A., Vignali, C., et al. 2010, *A&A*, 512, A34
- MacLeod, C. L., Ross, N. P., Lawrence, A., et al. 2016, *MNRAS*, 457, 389
- MacLeod, C. L., Green, P. J., Anderson, S. F., et al. 2019, *ApJ*, 874, 8
- McHardy, I. M., Cameron, D. T., Dwelly, T., et al. 2014, *MNRAS*, 444, 1469
- Netzer, H. 2019, *MNRAS*, 488, 5185
- Noda, H., & Done, C. 2018, *MNRAS*, 480, 3898
- Osterbrock, D. E., 1981, *ApJ*, 249, 462
- Parker, M. L., Schartel, N., Grupe, D., et al. 2019, *MNRAS*, 483, 88
- Peterson, B. M. 2014, *Space Sci. Rev.*, 183, 253
- Rivers, E., Markowitz, A., Duro, R., Rothschild, R., 2012, *ApJ*, 759, 63
- Risaliti, G., Young, M., Elvis, M., 2009, *ApJ*, 700, L6

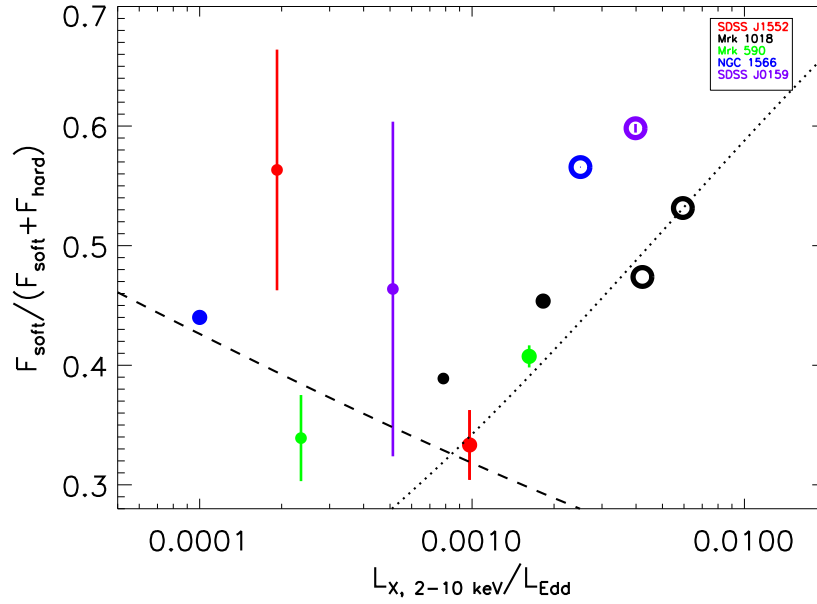


FIG. 5.— Variation of hardness ratio with the Eddington-scaled X-ray luminosity for changing-look AGNs. The F_{soft} and F_{hard} are the fluxes in 0.3-2 keV and 2-10 keV, respectively. Symbols with larger size represent the states with enhanced broad Balmer emission lines. Filled circles represent the optical spectral states of type 1.9/2, and open circles represent the type 1 states. The dashed line is the fit from Constantin et al. (2009), and the dotted line is the fit from Risaliti et al. (2009). The data for Mrk 1018, Mrk 590 and NGC 1566, and SDSS J015957.64+003310 are from the literatures (Longinotti et al. 2007; Denney et al. 2014; LaMassa et al. 2015; Noda & Done 2018; Parker et al. 2019).

- Ross, N. P., Ford, K. E. S., Graham, M., et al. 2018, MNRAS, 480, 4468
- Ruan, J. J., Anderson, S. F., Cales, S. L., et al. 2016, ApJ, 826, 188
- Ruan, J. J., Anderson, S. F., Eracleous, M., et al. 2019a, arXiv:1903.02553
- Ruan, J. J., Anderson, S. F., Eracleous, M., et al. 2019b, arXiv:1909.04676
- Rumbaugh, N., Shen, Y., Morganson, E., et al. 2018, ApJ, 854, 160
- Runco, J. N., Cosens, M., Bennert, V. N., et al. 2016, ApJ, 821, 33
- Runnoe, J. C., Cales, S., Ruan, J. J., et al. 2016, MNRAS, 455, 1691
- Qiao E. L., & Liu B. F., 2013, ApJ, 764, 2
- Schnorr-Müller, A., Davies, R. I., Korista, K. T., et al. 2016, MNRAS, 462, 3570
- Shappee, B. J., Prieto, J. L., Grupe, D., et al. 2014, ApJ, 788, 48
- Shen, Y., Brandt, W. N., Richards, G. T., et al. 2016, ApJ, 831, 7
- Sheng, Z., Wang, T., Jiang, N., et al. 2017, ApJL, 846, L7
- Sheng, Z., Wang, T., Jiang, N., et al. 2019, arXiv:1905.02904
- Śniegowska, M. & Czerny, B. 2019, arXiv, 190406767S
- Stern, D., McKernan, B., Graham, M. J., et al. 2018, ApJ, 864, 27
- Sobolewska, M. a., Papadakis, I. E., Done, C., Malzac, J., 2011, MNRAS, 417, 280
- Tohline, J. E., & Osterbrock, D. E. 1976, ApJL, 210, L117
- Trakhtenbrot, B., Ricci, C., Koss, M. J., et al. 2017, MNRAS, 470, 800
- Trakhtenbrot, B., Arcavi, I., MacLeod, C. L., et al. 2019, arXiv:1903.11084
- Trippe, M. L., Crenshaw, D. M., Deo, R. P., et al. 2010, ApJ, 725, 1749
- Sun, M. Y., Xue, Y. Q., Wang, J. X., Cai, Z. Y., Guo, H. X. 2018, ApJ, 866, 74
- Vanden Berk, D. E., Wilhite, B. C., Kron, R. G., et al. 2004, ApJ, 601, 692
- Vasudevan, R. V., & Fabian, A. C. 2007, MNRAS, 381, 1235
- Veilleux, S., & Osterbrock, D. E. 1987, ApJS, 63, 295
- Wang, J., Xu, D. W., & Wei, J. Y. 2018, ApJ, 858, 49
- Wang, J., Watarai, K., Mineshige, S., 2004, ApJ, 607, L107
- Wu, Q., & Gu, M. 2008, ApJ, 682, 212
- Xie, F. G., Zdziarski, A. A., Ma, R. Y., Yang, Q. X., 2016, MNRAS, 463, 2287
- Yao, S., Wu, X.-B., Ai, Y. L., et al. 2019, ApJS, 240, 6,
- Yang, Q., Wu, X.-B., Fan, X., et al. 2018, ApJ, 862, 109
- Yang, Q. X., Xie, F. G., Yuan, F., et al. 2015, MNRAS, 447, 1692
- Yuan, F., & Narayan, R., 2014, ARA&A, 52, 529
- Younes G., Porquet D., Sabra B., Reeves J. N., 2011, A&A, 530, 149
- Zhao, G., Zhao, Y. H., Chu, Y. Q., et al. 2012, RAA, 12, 723